Self-trapping of slow electrons in the energy domain

Maor Eldar,[1,2] Yiming Pan,[1] and Michael Krüger[1,2,*]

[1]*Department of Physics, Technion—Israel Institute of Technology, Haifa 32000, Israel*
[2]*Solid State Institute, Technion—Israel Institute of Technology, Haifa 32000, Israel*
(Dated: September 30, 2022)

The interaction of light and swift electrons has enabled phase-coherent manipulation and acceleration of electron wavepackets. Here we investigate this interaction in a new regime where low-energy electrons ($\sim$20-200 eV) interact with a phase-matched light field. Our analytical and numerical study shows that slow electrons are subject to strong confinement in the energy domain due to the non-vanishing curvature of the electron dispersion. The spectral trap is tunable and an appropriate choice of light field parameters can reduce the interaction dynamics to only two energy states. The capacity to trap electrons expands the scope of electron beam physics, free-electron quantum optics and quantum simulators.

The interaction between free electrons and light, resulting in a high degree of coherent control of the electron wavefunction, has been intensively studied during the past two decades [1–6]. The photonic part of the interaction can be achieved using different approaches, such as photon-induced near-field electron microscopy (PINEM, [1, 4, 7]), optical field discontinuities at interfaces [3, 8], dielectric laser acceleration (DLA, [9–11]), flat surfaces with phase-matched near-fields [5, 12], photonic cavities [6, 13] or ponderomotive acceleration [14]. The main signature of the interaction is the appearance of sidebands in the electron energy spectrum, enabling attosecond electron pulses [8, 15–19]. All these works have employed fast electrons (10-200 keV), enabling a straightforward understanding of much of the physics, primarily in the simplified picture of multi-level Rabi oscillations [4]. Here, the interaction with the optical field allows the electron to perform a quantum random walk on an infinite energy ladder. The multi-level Rabi oscillations model is based on approximations for fast electrons which include neglecting the electron momentum recoil (non-recoil approximation), applying the short-time interaction approximation without phase-matching, and neglecting the ponderomotive forces exerted by the strong light field. However, recent theory works have begun focusing on strong-field slow-electron interactions, for example via numerical study of strong off-resonant coupling at $\sim$0.1-1 keV [20] and inelastic ponderomotive scattering at $\sim$10 keV [21]. Recent advancements in low-energy electron microscopy and source development [22–30] are expected to enable first experimental studies of electron-light interactions in this novel regime.

In this Letter, we perform a theory study of the phase-matched interaction of slow electrons ($\sim$20-200 eV) with a strong optical field. We find that resonant interactions in this regime cause a strong confinement of the low-energy electron spectrum due to the non-vanishing curvature of the electron dispersion. The latter acts as a quadratic trapping potential in the energy domain, setting a limit to the quantum random walk of the electrons. We show that this trapping in the energy domain is tunable due to the competition of energy ladder hopping and electron dispersion which depends strongly on the frequency and strength of the optical driving field. Our findings demonstrate that the rich toolbox for manipulating free electrons with light is not restricted to fast electrons, but gives rise to interesting new phenomena in the regime of low-energy electrons, much beyond the multi-level Rabi picture.

In order to understand the strong-field dynamics of slow electrons, we perform a Floquet-Bloch analysis of the one-dimensional time-dependent Schrödinger equation. Key to our analysis is the electron's Hamiltonian given by $H_0 = E_0 + v_0(p - p_0) + (p - p_0)^2/(2\gamma^3 m)$, which we retrieve from expanding the relativistic dispersion to second order around the initial electron momentum p_0 (see Fig. 1(a)). Here m is the electron rest mass and $E_0 = \sqrt{m^2c^4 + p_0^2c^2} - mc^2$, $p_0 = \gamma m v_0$ and v_0 are the initial kinetic energy, momentum and velocity, respectively. γ is the Lorentz factor and c the speed of light. We further assume an optical field with phase-matched wavevector k_z along the propagation direction of the electron (see Fig. 1(b) for an illustration). The interaction Hamiltonian is given by $H_I = -\frac{e}{2\gamma m}(A \cdot p + p \cdot A) + \frac{e^2 A^2}{2\gamma m}$, where A is the optical field's vector potential and e the elementary charge. For a monochromatic field, the vector potential is given by $A(z, t) = -\frac{E_f}{\omega}\sin(\omega t - k_z z + \phi_0)$, where E_f, ω and ϕ_0 are the electric field amplitude, angular frequency and initial phase, respectively.

The electron-light interaction is imprinted on the resulting energy spectrum. After the electron enters the interaction region where the optical field is present it absorbs or emits an integer number of photons from the field, resulting in equally spaced energy states. Hence, encapsulating this spatiotemporal periodicity we employ the Floquet-Bloch ansatz $|\psi(t)\rangle = \sum_{n=-\infty}^{\infty} a_n(t)e^{-i\omega_n t}|k_n\rangle$ where n denotes the number of photons absorbed ($n > 0$) or emitted ($n < 0$) and a_n are the probability amplitudes corresponding to the respective energy-momentum states $|k_n\rangle$. Here $k_n = k_0 + nk_z$ and $\omega_n = \omega_0 + n\omega$ denote the wavenumber and angular frequency values, respectively. The electron's ini-
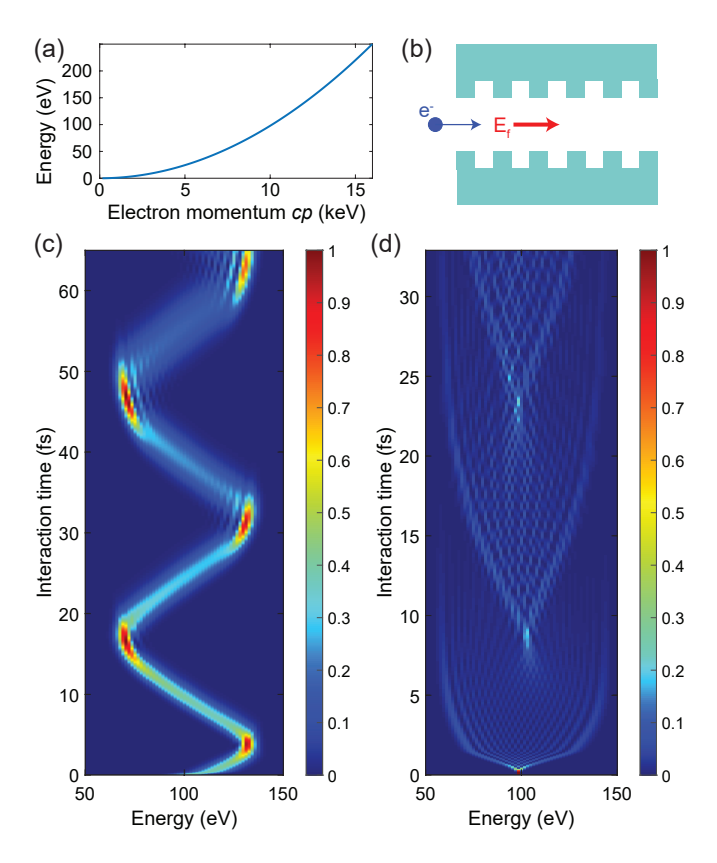
FIG. 1. Phase-matched low-energy electron light-matter interactions. (a) The electron dispersion for low-energy electrons displays a strong curvature. (b) Sketch of a possible setup. An electron is entering into a region of interaction with a phase-matched optical field. Phase-matching is achieved via dielectric gratings. (c) Evolution of the electron spectrum as a function of interaction time. The initial state is a localized wavepacket with an energy width corresponding to five photons $\Delta E \sim 7.5\,\mathrm{eV}$. (d) The same for a plane wave. In (c) and (d), the initial kinetic energy is set to $E_0 = 100\,\mathrm{eV}$. The optical field amplitude is $E_\mathrm{f} = 1\,\mathrm{V\,nm^{-1}}$, the photon energy is $\hbar\omega = 1.54\,\mathrm{eV}$ and the phase is $\phi_0 = 0$.

tial kinetic energy and momentum are given by $\hbar\omega_0 \equiv (\gamma-1)mc^2$ and $\hbar k_0 \equiv \gamma m v_0$, respectively. Substituting the ansatz into the Schrödinger equation we find

$$i\hbar \frac{\partial a_n(t)}{\partial t} = -\left[n\hbar(\omega - v_0 k_z) - n^2 \frac{(\hbar k_z)^2}{2m} + U_\mathrm{p} \right] a_n(t)$$
$$+\delta\left((k_{n+1} - \frac{k_z}{2})a_{n+1}(t)e^{i\phi} + (k_{n-1} + \frac{k_z}{2})a_{n-1}(t)e^{-i\phi} \right)$$
$$-\frac{U_\mathrm{p}}{2}\left(a_{n+2}(t)e^{i2\phi_0} + a_{n-2}(t)e^{-i2\phi_0} \right),$$
$$(1)$$

where $U_\mathrm{p} = e^2 E_\mathrm{f}^2/(4m\omega^2)$ is the ponderomotive energy, $\delta = e\hbar E_\mathrm{f}/(2m\omega)$ and $\phi = \phi_0 + \frac{\pi}{2}$. Eq. 1 reveals several intriguing and unique characteristics of the slow electron-light interaction, as we will explain below.

In order to resonantly couple the slow electron and

the field, we require the conservation of both energy and momentum for single photon emission or absorption by the electron at the quantum level, resulting in the phase-matching condition of equal electron (group) velocity and optical field (phase) velocity [31]. This phase-matching condition also holds true for low-energy electrons (see Supplemental Material [32]). We note that it is challenging to achieve phase-matching for slow electrons ($\approx 100\,\mathrm{eV}$) since it requires a significant reduction of the phase velocity of the optical field, but it is not impossible. For instance, DLA requires a grating structure with a period of 15 nm for 100 eV electrons and 800 nm wavelength. Alternatively, the use of plasmonic metamaterials [33] or materials with very high refractive index ($n \approx 50$), such as $SrTiO_3$ at low temperatures [34], can generate optical waves with an extremely small phase velocity.

The A^2 ponderomotive term of the interaction Hamiltonian is reflected in the third line of Eq. 1, permitting two-photon exchanges in each interaction event. It becomes more important for slow electrons since the competing linear interaction term $p \cdot A$ decreases with velocity. However, even for a 50 eV electron, strong electric fields with amplitudes on the order of $10\,\mathrm{V\,nm^{-1}}$ have to be applied to make the ponderomotive term comparable to the $p \cdot A$ term. In contrast to free-space ponderomotive schemes [14, 21, 35], material damage thresholds limit the applicable field intensity. Under this limitation, a strong ponderomotive effect can still be reached if the electron kinetic energy approaches the single photon energy, $eE_\mathrm{f}/\omega \approx p_0$ (see Supplemental Material [32]).

The second characteristic of slow-electron strong-field interaction is the breakdown of the non-recoil approximation. For fast electrons, the detuning in momentum recoil owing to photon absorption and emission may be neglected, as explicitly represented by $k_{n+1} \approx k_{n-1} \approx k_0$ [4]. However, this is no longer true for slow electrons. In order to reveal this, we focus on the ratio $|\Delta v|/v_0$, where Δv is the velocity change caused by a single photon exchange. For an electron with $E_0 = 50\,\mathrm{eV}$ and a photon energy $\hbar\omega = 1.54\,\mathrm{eV}$, we find $|\Delta v|/v_0 = \sqrt{\hbar\omega/E_0} \approx 10^{-1}$. In contrast, for a fast electron of $E_0 = 200\,\mathrm{keV}$ we find $|\Delta v|/v_0 \approx 10^{-3}$, hence the detuning can be neglected. The breakdown of the non-recoil approximation amounts to an effective symmetry breaking between absorption and emission, which is most pronounced at higher orders of photon scattering and manifests as a slightly altered coupling constant at the level of single photon exchange. In addition, we find an asymmetric evolution pattern in the electron spectrum when electrons and light are not phase-matched. This leads to a different group velocity dispersion for emission and absorption sidebands, resulting in asymmetric Bloch-type oscillations (see Supplemental Material [32]).

The first line of Eq. 1 reveals two potentials acting on the time evolution of the sideband momentum states,

$n\hbar(\omega - v_0 k_z)$ and $-(n\hbar k_z)^2/(2m)$. The first potential term is linear in n and results from the mismatch between electron group velocity and light field phase velocity. Under the condition $\omega \neq v_0 k_z$, this phase mismatch acts effectively as a linear potential on a synthetic frequency space resulting in Bloch oscillation dynamics in the energy spectrum as reported previously for fast free electrons [36, 37], which lead to Wannier-Stark localization [38]. However, when we introduce phase-matching through $\omega = v_0 k_z$, the linear term vanishes and we are left with the quadratic potential term. The latter is only significant for slow electrons and acts as a confining potential for the electron's spectral evolution. Figures 1(c) and (d) displays the population probability of the sideband momentum states as function of interaction time obtained from numerical solutions of Eq. 1. We show the results for two initial conditions, a localized Gaussian wavepacket (Fig. 1(c)) and a single energy (plane wave, Fig. 1(d)), both centered at 100 eV initial kinetic energy. The field strength is set to $E_{\mathrm{f}} = 1\,\mathrm{V\,nm^{-1}}$ and the single photon energy is $\hbar\omega = 1.54\,\mathrm{eV}$. We observe a spectral evolution exhibiting strong confinement and oscillations. For the electron wavepacket, we find that the spectral evolution follows a classical Lorentz-like trajectory for a charged particle in an electric field. In contrast, for a plane-wave electron we see spectral broadening to a superposition state, which subsequently ceases to expand and suddenly collapses to a single sideband. In both cases, we observe a spectral asymmetry in the energy spectrum as a small but noticeable difference ($\Delta n \approx 3$) between the maximally populated energy states of absorption and emission. This asymmetry is a signature of the non-vanishing curvature of the electron dispersion at low energies and accumulates across successive photon scattering events.

In order to analytically capture the basic underlying physics in Fig. 1, we lay aside the asymmetry in absorption and emission by applying the approximation $k_{n+1} \approx k_{n-1} \approx k_0$ and neglect ponderomotive effects. We are thus left with a simplified equation,

$$i\hbar\frac{\partial a_n}{\partial t} = \beta n^2 a_n + \kappa a_{n+1} + \kappa^* a_{n-1}, \qquad (2)$$

where $\beta = \frac{(\hbar k_z)^2}{2m}$ and $\kappa = \frac{eE_{\mathrm{f}}\hbar k_0}{2m\omega}e^{i(\phi_0+\pi/2)}$. By relating β to the electron and light field parameters under phase-matching, we find $\beta \approx \frac{1}{4}(\hbar\omega)^2/E_0$.

From Eq. 2 we can easily read the two competing processes that govern the spectral dynamics, namely harmonic oscillations and hopping. In analogy to solid-state terminology, we refer to the two terms on the r.h.s. of Eq. 2 as quadratic on-site potential ($n^2\beta$) and nearest-neighbour hopping (κ). Both parameters depend on the optical field parameters and the electron's energy dispersion. We note that the evolution of the electron spectrum governed by Eq. 2 is analogous to the Schrödinger equation for atomic diffraction [39] and the transversal
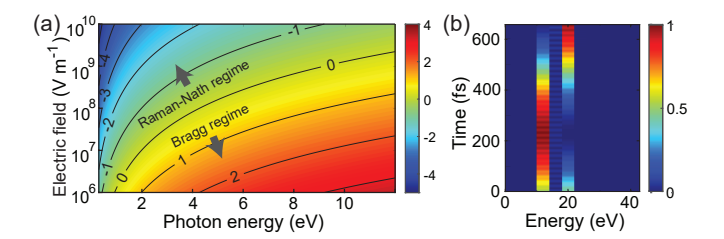

FIG. 2. (a) Transition between Raman-Nath and Bragg regimes. We show $\log\rho$ as a function of photon energy $\hbar\omega$ and electric field strength E_{f}. The initial electron energy is 100 eV. (b) Spectral evolution in the Bragg regime for two initial energy components (12 eV and 20 eV), photon energy $\hbar\omega = 4\,\mathrm{eV}$ and $E_{\mathrm{f}} = 1 \times 10^8\,\mathrm{V\,nm^{-1}}$ ($\rho \approx 10$). We observe oscillations between the initial energy components.

Kapitza-Dirac effect for electron diffraction [40]. In order to distinguish the relative contribution of the two effects we invoke the Nath parameter, $\rho = \beta/\kappa$ [41]. In Fig. 2(a), we show $\log\rho$ as a function of photon energy and field strength. For $\rho \ll 1$, the hopping dominates, indicating the Raman-Nath regime, whereas for $\rho \gg 1$ we find the Bragg regime [42]. In the following, we will discuss both regimes and their effects on electron spectral evolution.

We first discuss the Raman–Nath regime ($\rho \ll 1$) which is reached when the hopping energy is much larger than the on-site energy. We can thus treat the latter as a perturbation. For instance, a slow electron with kinetic energy of 100 eV can reach this regime while interacting with an electric field with wavelength 800 nm and $E_{\mathrm{f}} = 1\,\mathrm{V\,nm^{-1}}$, yielding $\rho \sim 10^{-3}$. The unperturbed equation then reads: $i\hbar\frac{\partial a_n(t)}{\partial t} = \kappa a_{n+1}(t) + \kappa^* a_{n-1}(t)$, which has a known analytical solution in the form of a Bessel function of the first kind, $a_n(t) = J_n(\frac{2|\kappa|}{i\hbar}t)e^{in\phi_0}$ (see Supplemental Material [32]). We obtain the probability $P_n(t)$ of locating the electron at a certain sideband as $P_n(t) = |J_n(\frac{2|\kappa|}{i\hbar}t)|^2$. The quantum coherent dynamics given by the Bessel function solution entail a symmetric diffraction pattern, as observed in Fig. 1(b) for early times $0 - 2$ fs, in full analogy to PINEM with fast electrons [4]. However, at later times ($2 - 8$ fs), the rapid expansion is considerably slowed down as the confining term ($\propto n^2$) becomes significant at these high sidebands. Physically, this is the result of energy–momentum conservation being violated at high photon scattering orders, due to the growing phase mismatch between light (linear dispersion) and free electron (quadratic dispersion). As a result, all trajectories self-collapse in close vicinity of the initial momentum state at around $\sim 8 - 9$ fs and the evolution pattern then repeats periodically throughout the interaction time.

For $\rho \gg 1$ where the hopping is smaller then the on-site potential term, we find the Bragg regime [40]. As shown in Fig. 2(a), entering the Bragg regime necessitates relatively weak electric fields ($\sim 10^6 - 10^8\,\mathrm{V\,m^{-1}}$)

and high-energy photons ($\hbar\omega \sim 4-20\,\text{eV}$). In this regime, fewer sideband orders are populated compared to the Raman–Nath regime, which can be understood as the quantum electron optics analog of optical Bragg diffraction but occurring here in the electron spectrum. The on-site term $\propto n^2$ invokes a symmetry between photon emission and absorption scattering orders ($n, -n$). Therefore, even with a small hopping term of the Bragg regime, there exists a non-negligible coupling between these sidebands. For an initial spectrum containing only a single sideband, the Bragg regime can offer the strongest possible confinement involving only two sidebands, i.e., a coherent splitting of the electron spectrum much like a diffraction grating in optics. The dynamics takes the form of periodic oscillation between the two energy components, an effect known in neutron diffraction as Pendellösung oscillations [43], and was also observed in atom optics experiments [44]. A pure quantum effect occurs if the photon energy is on the order of the electron energy. Here, the slow electron populates only a few sidebands within a strong spectral confinement. The quantization grid in the electron phase space is comparable to its volume, therefore already exchanging a small number of photons leads to a large energy-momentum violation (large phase mismatch) and therefore eliminates higher sidebands (see Fig. 2(b) for an example). Interestingly, for free-electron lasers a similar transition to a quantum regime was found [45].

At this moment, we can control and manipulate the spectral confinement of the laser-modulated free electrons, enabling their trapping in the energy domain. This is achievable because the preceding analysis clarifies both the electron and light field parameters in each regime, as we will now demonstrate in detail. From now on throughout our study we stay in the Raman-Nath regime ($E_\text{f} \approx 1\,\text{V}\,\text{nm}^{-1}$ and $\hbar\omega = 1.54\,\text{eV}$). For our spectral trap, it is reasonable to define an effective trap width. We define the width as the energy difference between the minimum and the maximum populated sidebands. The spectral trap depends on the field parameters and the initial electron energy distribution. In Fig. 3(a), we show the dependence of the effective trap width on the electron energy for the wavepacket and the plane wave from Fig. 1(c) and (d), respectively, with the phase-matching adjusted to each energy. Not surprisingly, an increase in energy leads to weaker influence of the quadratic potential and therefore weaker trapping. A similar increase in width is reached by increasing the optical field strength, which enhances the hopping (see Fig. 3(b)). The definition of κ reveals another parameter that influences the trap width, the optical phase ϕ_0 with respect to the beginning of the interaction when the electron enters the optical field. This dependence can be explained with an analogy to the classical harmonic oscillator, for which the largest energy transfer between the driving force and mass occurs when the phase difference (time difference)
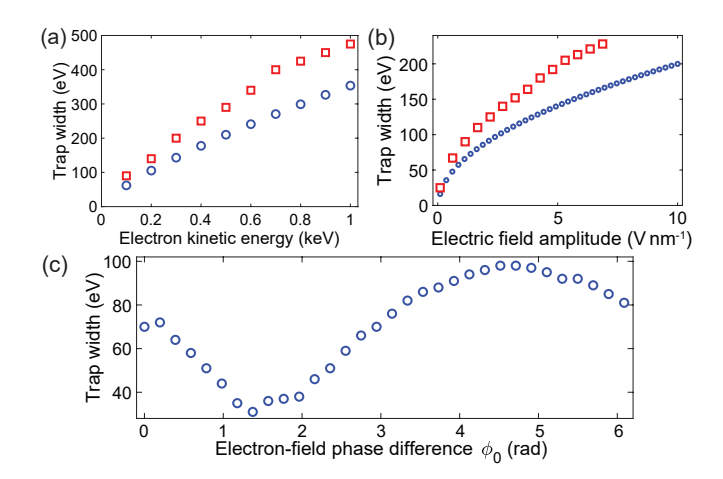

FIG. 3. Parameter dependence of the trap width. (a) Dependence on electron energy for $E_\text{f} = 1\,\text{V}\,\text{nm}^{-1}$, $\hbar\omega = 1.54\,\text{eV}$ and $\phi_0 = 0$. The phase-matching is adjusted for each energy. Blue circles: Initial wavepacket as in Fig. 1(c). Red squares: Plane wave. (b) The same as (a), but as a function of electric field amplitude for $100\,\text{eV}$ electrons. (c) Dependence of the trap depth on the relative phase between electron and light field for the wavepacket.

between the two is $\frac{\pi}{2}$. This is consistent with our findings, where we find the maximum trap width for $\frac{\pi}{2}$ and a minimum for $-\frac{\pi}{2}$ (see Fig. 3(c)).

In Figure 1(c), we notice the appearance of spectral Airy-like fringes forming at intermediate and long evolution times in the vicinity of the trap edges, i.e., at the turning points for a confined and oscillatory localized wavepacket. These fringes are due to an interference pattern which emerges from the different phases accumulated by the set of initially occupied sideband states. The difference in phase accumulation by the different plane waves is strongest in the vicinity of the trap edges. A few oscillation cycles are required to develop a pronounced fringe pattern. This may be demonstrated by initializing the wavepacket closer to the quadratic potential minimum by altering the phase difference, which results in longer interaction times for the fringes to form and vice versa.

In conclusion, our work explores the spectral dynamics of the resonant interaction of a low-energy electron with a strong light field. With the help of analytical models and numerical simulations, we find new spectral features appearing as the interaction evolves. Particularly, we report a confinement of the electron spectrum induced by the curvature of the electron dispersion which is not accessible for fast electrons. Tunable with the help of the optical field parameters, effective trap widths ranging from few tens to few hundreds electron volts can be achieved. Our findings can be highly useful for electron manipulation. First, a confinement to only a few energy sidebands in the Bragg regime offers a natural truncation of the infinite Hilbert space of the multi-level Rabi

ladder, allowing for adiabatic eliminations that enable us to get rid of undesired sidebands and higher-order photon transitions. Second, the finite Hilbert space as a synthetic spatial dimension can be then of aid for carrying out quantum simulations and computations utilizing coherent laser-electron interactions, as proposed recently for fast electrons [37]. Finally, the dynamical confinement in the low-energy regime can help controlling the maximum energy transfer for laser-driven charged-particle acceleration, the minimum bunching size of an electron beam and the maximum photon energy produced in free-electron radiation.

———————————

* Corresponding author: krueger@technion.ac.il

[1] B. Barwick, D. J. Flannigan, and A. H. Zewail, Photon-induced near-field electron microscopy, Nature **462**, 902 (2009).

[2] F. J. García de Abajo, Optical excitations in electron microscopy, Rev. Mod. Phys. **82**, 209 (2010).

[3] F. O. Kirchner, A. Gliserin, F. Krausz, and P. Baum, Laser streaking of free electrons at 25 keV, Nat. Phot. **8**, 52 (2014).

[4] A. Feist, K. E. Echternkamp, J. Schauss, S. V. Yalunin, S. Schäfer, and C. Ropers, Quantum coherent optical phase modulation in an ultrafast transmission electron microscope, Nature **521**, 200 (2015).

[5] R. Dahan, S. Nehemia, M. Shentcis, O. Reinhardt, Y. Adiv, X. Shi, O. Be'er, M. H. Lynch, Y. Kurman, K. Wang, and I. Kaminer, Resonant phase-matching between a light wave and a free-electron wavefunction, Nat. Phys. **16**, 1123 (2020).

[6] J.-W. Henke, A. S. Raja, A. Feist, G. Huang, G. Arend, Y. Yang, F. J. Kappert, R. N. Wang, M. Möller, J. Pan, J. Liu, O. Kfir, C. Ropers, and T. J. Kippenberg, Integrated photonics enables continuous-beam electron phase modulation, Nature **600**, 653 (2021).

[7] R. Shiloh, T. Chlouba, and P. Hommelhoff, Quantum-coherent light-electron interaction in a scanning electron microscope, Phys. Rev. Lett. **128**, 235301 (2022).

[8] Y. Morimoto and P. Baum, Diffraction and microscopy with attosecond electron pulse trains, Nat. Phys. **14**, 252 (2018).

[9] J. Breuer and P. Hommelhoff, Laser-based acceleration of nonrelativistic electrons at a dielectric structure, Phys. Rev. Lett. **111**, 134803 (2013).

[10] E. Peralta, K. Soong, E. R. England, R. J.and Colby, Z. Wu, B. Montazeri, C. McGuinness, J. McNeur, K. J. Leedle, D. Walz, E. Sozer, B. Cowan, B. Schwartz, G. Travish, and R. L. Byer, Demonstration of electron acceleration in a laser-driven dielectric microstructure, Nature **503**, 91 (2013).

[11] Y. Adiv, K. Wang, R. Dahan, P. Broaddus, Y. Miao, D. Black, K. Leedle, R. L. Byer, O. Solgaard, R. J. England, and I. Kaminer, Quantum nature of dielectric laser accelerators, Phys. Rev. X **11**, 041042 (2021).

[12] M. Kozák, P. Beck, H. Deng, J. McNeur, N. Schönenberger, C. Gaida, F. Stutzki, M. Gebhardt, J. Limpert, A. Ruehl, I. Hartl, O. Solgaard, J. S. Harris, R. L. Byer, and P. Hommelhoff, Acceleration of sub-relativistic electrons with an evanescent optical wave at a planar interface, Opt. Express **25**, 19195 (2017).

[13] O. Kfir, H. Lourenço-Martins, G. Storeck, M. Sivis, T. R. Harvey, T. J. Kippenberg, A. Feist, and C. Ropers, Controlling free electrons with optical whispering-gallery modes, Nature **582**, 46 (2020).

[14] M. Kozák, T. Eckstein, N. Schönenberger, and P. Hommelhoff, Inelastic ponderomotive scattering of electrons at a high-intensity optical travelling wave in vacuum, Nat. Phys. **14**, 121 (2018).

[15] K. E. Priebe, C. Rathje, S. V. Yalunin, T. Hohage, A. Feist, S. Schäfer, and C. Ropers, Attosecond electron pulse trains and quantum state reconstruction in ultrafast transmission electron microscopy, Nat. Phot. **11**, 793 (2017).

[16] M. Kozák, All-optical scheme for generation of isolated attosecond electron pulses, Phys. Rev. Lett. **123**, 203202 (2019).

[17] D. S. Black, U. Niedermayer, Y. Miao, Z. Zhao, O. Solgaard, R. L. Byer, and K. J. Leedle, Net acceleration and direct measurement of attosecond electron pulses in a silicon dielectric laser accelerator, Phys. Rev. Lett. **123**, 264802 (2019).

[18] N. Schönenberger, A. Mittelbach, P. Yousefi, J. McNeur, U. Niedermayer, and P. Hommelhoff, Generation and characterization of attosecond microbunched electron pulse trains via dielectric laser acceleration, Phys. Rev. Lett. **123**, 264803 (2019).

[19] Y. Morimoto and P. Baum, Single-cycle optical control of beam electrons, Phys. Rev. Lett. **125**, 193202 (2020).

[20] N. Talebi, Strong interaction of slow electrons with near-field light visited from first principles, Phys. Rev. Lett. **125**, 080401 (2020).

[21] M. Kozák and T. Ostatnickỳ, Asynchronous inelastic scattering of electrons at the ponderomotive potential of optical waves, Phys. Rev. Lett. **129**, 024801 (2022).

[22] P. Hommelhoff, Y. Sortais, A. Aghajani-Talesh, and M. A. Kasevich, Field emission tip as a nanometer source of free electron femtosecond pulses, Phys. Rev. Lett. **96**, 077401 (2006).

[23] C. Ropers, D. R. Solli, C. P. Schulz, C. Lienau, and T. Elsaesser, Localized multiphoton emission of femtosecond electron pulses from metal nanotips, Phys. Rev. Lett. **98**, 043907 (2007).

[24] B. Barwick, C. Corder, J. Strohaber, N. Chandler-Smith, C. Uiterwaal, and H. Batelaan, Laser-induced ultrafast electron emission from a field emission tip, New J. Phys. **9**, 142 (2007).

[25] M. Krüger, M. Schenk, and P. Hommelhoff, Attosecond control of electrons emitted from a nanoscale metal tip, Nature **475**, 78 (2011).

[26] E. Quinonez, J. Handali, and B. Barwick, Femtosecond photoelectron point projection microscope, Rev. Sci. Instr. **84**, 103710 (2013).

[27] D. Ehberger, J. Hammer, M. Eisele, M. Krüger, J. Noe,

A. Högele, and P. Hommelhoff, Highly coherent electron beam from a laser-triggered tungsten needle tip, Phys. Rev. Lett. **114**, 227601 (2015).

[28] J. Vogelsang, G. Hergert, D. Wang, P. Groß, and C. Lienau, Observing charge separation in nanoantennas via ultrafast point-projection electron microscopy, Light: Sci. Appl. **7**, 55 (2018).

[29] J. Vogelsang, N. Talebi, G. Hergert, A. Wöste, P. Groß, A. Hartschuh, and C. Lienau, Plasmonic-nanofocusing-based electron holography, ACS Photon. **5**, 3584 (2018).

[30] M. Eldar, S. Abo-Toame, and M. Krüger, Sub-optical-cycle electron pulse trains from metal nanotips, J. Phys. B: At. Mol. Opt. Phys. **55**, 074001 (2022).

[31] S. T. Park, M. Lin, and A. H. Zewail, Photon-induced near-field electron microscopy (PINEM): theoretical and experimental, New J. Phys. **12**, 123028 (2010).

[32] See Supplemental Material at [URL will be inserted by publisher] for complete derivations and supplementary figures.

[33] K. L. Tsakmakidis, O. Hess, R. W. Boyd, and X. Zhang, Ultraslow waves on the nanoscale, Science **358**, eaan5196 (2017).

[34] T. Sakudo and H. Unoki, Dielectric properties of $SrTiO_3$ at low temperatures, Phys. Rev. Lett. **26**, 851 (1971).

[35] D. L. Freimund, K. Aflatooni, and H. Batelaan, Observation of the Kapitza–Dirac effect, Nature **413**, 142 (2001).

[36] A. Pick, O. Reinhardt, Y. Plotnik, L. J. Wong, and I. Kaminer, Bloch oscillations of a free electron in a strong field, in *CLEO: QELS_Fundamental Science* (Optica Publishing Group, 2018) pp. FF1E–5.

[37] Y. Pan, B. Zhang, and D. Podolsky, Synthetic dimensions using ultrafast free electrons, arXiv preprint arXiv:2207.07010 (2022).

[38] G. H. Wannier, Wave functions and effective hamiltonian for Bloch electrons in an electric field, Phys. Rev. **117**, 432 (1960).

[39] P. Meystre and M. O. Scully, *Quantum optics* (Springer, 2021).

[40] H. Batelaan, Colloquium: Illuminating the Kapitza-Dirac effect with electron matter optics, Rev. Mod. Phys. **79**, 929 (2007).

[41] N. N. Nath, The diffraction of light by supersonic waves, in *Proc. Indian Acad. Sci. Sect. A*, Vol. 8 (1938) pp. 499–503.

[42] M. Moharam and L. Young, Criterion for Bragg and Raman-Nath diffraction regimes, Appl. Opt. **17**, 1757 (1978).

[43] C. G. Shull, Observation of Pendellösung fringe structure in neutron diffraction, Phys. Rev. Lett. **21**, 1585 (1968).

[44] P. J. Martin, B. G. Oldaker, A. H. Miklich, and D. E. Pritchard, Bragg scattering of atoms from a standing light wave, Phys. Rev. Lett. **60**, 515 (1988).

[45] P. Kling, E. Giese, R. Endrich, P. Preiss, R. Sauerbrey, and W. P. Schleich, What defines the quantum regime of the free-electron laser?, New J. Phys. **17**, 123019 (2015).

Self-trapping of slow electrons in the energy domain: Supplemental material

Maor Eldar[1,2], Yiming Pan[1], Michael Krüger[1,2]

September 30, 2022

[1]Department of Physics, Technion—Israel Institute of Technology, Technion City, 32000 Haifa, Israel

[2]Solid State Institute, Technion—Israel Institute of Technology, Haifa 32000, Israel

Table of contents

1 General tight-binding-approximated equation using the Floquet-Bloch theorem

In accordance with our description of the slow-electron resonant interaction setup in the main text, we begin with the time-dependent Schrödinger equation:

$$i\hbar\frac{\partial}{\partial t}|\psi(t)\rangle = (\hat{H}_0 + \hat{H}_\mathrm{I})|\psi(t)\rangle, \tag{S1}$$

in which $|\psi(t)\rangle$ is the electron wavevector, $\hat{H}_0$ is the free-electron Hamiltonian and $\hat{H}_\mathrm{I}$ is the electron-light interaction Hamiltonian. A Taylor expansion of the relativistic energy dispersion to second order (see section 3 for derivation) leads to

$$H_0 = E_0 + v_0(p - p_0) + \frac{(p - p_0)^2}{2\gamma^3 m}. \tag{S2}$$

Notice that henceforth we omit operator signs for convenience. The electron's initial kinetic energy is $E_0 = \sqrt{m^2c^4 + p_0^2c^2} - mc^2$, where p_0 is its initial momentum, c the vacuum speed of light, γ is the Lorentz factor, e is the elementary charge and m is the electron's rest mass. The interaction Hamiltonian results from the minimal coupling by substituting p by $p - eA$,

$$H_\mathrm{I} = -\frac{e}{2\gamma m}\big[A \cdot p + p \cdot A\big] + \frac{e^2A^2}{2\gamma m}, \tag{S3}$$

where for our concern the laser-induced vector potential along electron propagation direction is given by $A = A(z,t) = -\frac{E_f}{\omega}\sin(\omega t - k_z z + \phi_0)$. Here E_f, ω and ϕ_0 are the electric field amplitude, angular frequency and initial phase, respectively. k_z is the optical wavevector along the propagation direction of the electron.

Considering the spatiotemporal periodicity of the vector potential, we employ the Floquet-Bloch ansatz:

$$|\psi(z,t)\rangle = \sum_{n=-\infty}^{\infty} a_n(t)e^{-i\omega_n t}|k_n\rangle, \text{ or}$$

$$\psi(z,t) = \sum_{n=-\infty}^{\infty} a_n(t)e^{-i(w_n t - k_n z)}, \tag{S4}$$

where we define

$$\omega_n = \omega_0 + n\omega,$$
$$k_n = k_0 + nk_z,$$
$$\omega_0 = E_0/\hbar,$$
$$k_0 = p_0\hbar.$$

We substitute Eq. S4 into Eq. S1. First we derive the left-hand side:

$$i\hbar \sum_n e^{-i(\omega_n t - k_n z)}\left(-i\omega_n + \frac{\partial}{\partial t}\right)a_n(t) = \sum_n e^{-i(\omega_n t - k_n z)}\left(\hbar\omega_n + i\hbar\frac{\partial}{\partial t}\right)a_n(t),$$

and the right-hand side takes the form:

$$\sum_{n=-\infty}^{\infty}\left(E_0 + v_0(p-p_0) + \frac{(p-p_0)^2}{2\gamma^3 m} - \frac{e}{2\gamma m}\left[A\cdot p + p\cdot A\right] + \frac{e^2 A^2}{2\gamma m}\right)a_n(t)e^{-i(\omega_n t - k_n z)}.$$

We now evaluate each term of the right hand side individually. First, we calculate the H_0 term:

$$H_0|\psi(t)\rangle = \sum_n \left(E_0 + v_0 n\hbar k_z + \frac{(n\hbar k_z)^2}{2\gamma^3 m}\right)a_n(t)e^{-i(\omega_n t - k_n z)}, \tag{S5}$$

where we used the de-Broglie relation, $p = \hbar k$. Next, we calculate the linear term $A\cdot p + p\cdot A$:

$$H_I|\psi(t)\rangle = -\frac{e}{2\gamma m}\left(A\cdot p + p\cdot A\right)\sum_n a_n(t)e^{-i\omega_n t}|k_n\rangle.$$

Recalling $p = -i\hbar\frac{\partial}{\partial z}$ and $I = \int dz|z\rangle\langle z|$, we continue

$$H_I|\psi(t)\rangle = \frac{e}{2\gamma m}(-Ai\hbar\frac{\partial}{\partial z} - i\hbar\frac{\partial}{\partial z}A(z,t))\sum_{n=-\infty}^{\infty}a_n(t)e^{-i\omega_n t}\int dz|z\rangle\langle z|k_n\rangle$$

$$= -\hbar\frac{eA_0}{\gamma m}\sum_n[(k_n - i\frac{\partial}{\partial z})a_n(t)]e^{-i\omega_n t}\int dz\, e^{-ik_n z}\sin(\omega t - k_z z + \phi_0)|z\rangle$$

$$- i\hbar\frac{eA_0}{2\gamma m}k_z\sum_n a_n(t)e^{-i\omega_n t}\int dz\, e^{ik_n z}\cos(\omega t - k_z z + \phi_0), \tag{S6}$$

where we labeled $A_0 = -\frac{E_f}{\omega}$ and applied the projection $\langle z|k_n\rangle = e^{ik_n z}$. We now use the known decomposition:

$$\sin(\omega t - k_z z + \phi_0) = -\frac{i}{2}[e^{i(\omega t - k_z z + \phi_0)} - e^{-i(\omega t - k_z z + \phi_0)}],$$

$$\cos(\omega t - k_z z + \phi_0) = \frac{1}{2}[e^{i(\omega t - k_z z + \phi_0)} + e^{-i(\omega t - k_z z + \phi_0)}].$$

By inserting this decomposition into Eq. S6 we obtain:

$$H_{\mathrm{I}}|\psi(t)\rangle = i\hbar\frac{eA_0}{\gamma m}\sum_n[(k_n - \frac{k_z}{2} - i\frac{\partial}{\partial z})a_n(t)]\int dz\, e^{-i(\omega_{n-1}t - k_{n-1}z - \phi_0)}|z\rangle$$

$$- i\hbar\frac{eA_0}{\gamma m}\sum_n[(k_n + \frac{k_z}{2} - i\frac{\partial}{\partial z})a_n(t)]\int dz\, e^{-i(\omega_{n+1}t - k_{n+1}z - \phi_0)}|z\rangle.$$

Inserting the identity operator $I = \frac{1}{2\pi}\int dk|k\rangle\langle k|$ we find

$$H_{\mathrm{I}}|\psi(t)\rangle = i\hbar\frac{eA_0}{\gamma m}\sum_n[(k_n - \frac{k_z}{2} - i\frac{\partial}{\partial z})a_n(t)]\frac{1}{2\pi}\int dz\int dk\, e^{-ikz}e^{-i(\omega_{n-1}t - k_{n-1}z - \phi_0)}|k\rangle$$

$$- i\hbar\frac{eA_0}{\gamma m}\sum_n[(k_n + \frac{k_z}{2} - i\frac{\partial}{\partial z})a_n(t)]\frac{1}{2\pi}\int dz\int dk\, e^{-ikz}e^{-i(\omega_{n+1}t - k_{n+1}z - \phi_0)}|k\rangle$$

$$= i\hbar\frac{eA_0}{\gamma m}\sum_n[(k_n - \frac{k_z}{2} - i\frac{\partial}{\partial z})a_n(t)]\frac{1}{2\pi}\int dk\left[\int dz\, e^{-i(k - k_{n-1})z}\right]e^{-i(\omega_{n-1}t - \phi_0)}|k\rangle$$

$$- i\hbar\frac{eA_0}{\gamma m}\sum_n[(k_n + \frac{k_z}{2} - i\frac{\partial}{\partial z})a_n(t)]\frac{1}{2\pi}dk\left[\int dz\, e^{-i(k - k_{n+1})z}\right]e^{-i(\omega_{n+1}t - \phi_0)}|k\rangle$$

$$= i\hbar\frac{eA_0}{\gamma m}\sum_n[(k_n - \frac{k_z}{2} - i\frac{\partial}{\partial z})a_n(t)]\frac{1}{2\pi}\int dk\,\delta(k - k_{n-1})e^{-i(\omega_{n-1}t - \phi_0)}|k\rangle$$

$$- i\hbar\frac{eA_0}{\gamma m}\sum_n[(k_n + \frac{k_z}{2} - i\frac{\partial}{\partial z})a_n(t)]\frac{1}{2\pi}dk\int dk\,\delta(k - k_{n+1})e^{-i(\omega_{n+1}t - \phi_0)}|k\rangle$$

$$= i\hbar\frac{eA_0}{\gamma m}\sum_n[(k_n - \frac{k_z}{2} - i\frac{\partial}{\partial z})a_n(t)]\frac{1}{2\pi}e^{-i(\omega_{n-1}t - \phi_0)}|k_{n+1}\rangle$$

$$- i\hbar\frac{eA_0}{\gamma m}\sum_n[(k_n + \frac{k_z}{2} - i\frac{\partial}{\partial z})a_n(t)]\frac{1}{2\pi}e^{-i(\omega_{n+1}t - \phi_0)}|k_{n+1}\rangle.$$

Next, we shift the dummy index n to find:

$$H_{\mathrm{I}}|\psi(t)\rangle = i\hbar\frac{eA_0}{\gamma m}\sum_n e^{-i\omega_n t}[a_{n+1}(t)(k_{n+1} - \frac{k_z}{2})e^{i\phi_0} - a_{n-1}(t)(k_{n-1} + \frac{k_z}{2})e^{-i\phi_0}]|k_n\rangle$$

$$+ \hbar\frac{eA_0}{\gamma m}\sum_n e^{-i\omega_n t}[e^{i\phi_0}\frac{\partial}{\partial z}a_{n+1}(z,t) - e^{-i\phi_0}\frac{\partial}{\partial z}a_{n-1}(z,t)]|k_n\rangle.$$

Assuming a_n is slowly varying, we neglect second order derivatives and are thus left with:

$$H_{\mathrm{I}}|\psi(t)\rangle \approx i\hbar\frac{eA_0}{\gamma m}\sum_n e^{-i\omega_n t}[a_{n+1}(t)(k_{n+1} - \frac{k_z}{2})e^{i\phi_0} - a_{n-1}(t)(k_{n-1} + \frac{k_z}{2})e^{-i\phi_0}]|k_n\rangle. \tag{S7}$$

Next, we derive the ponderomotive term $\frac{(eA)^2}{2\gamma m}$:

3

$$\frac{e^2 E_{\mathrm{f}}^2}{2\gamma m\omega^2} \sum_n (\sin(\omega t - k_z z + \phi_0))^2 a_n(t) e^{-i(\omega_n t - k_n z)}$$

$$= \frac{e^2 E_{\mathrm{f}}^2}{2\gamma m\omega^2} \sum_n \left\{ \frac{e^{2i(\omega t - k_z z + \phi_0)} + e^{-2i(\omega t - k_z z + \phi_0)} - 2}{-4} \right\} e^{-i(\omega_n t - k_n z)} a_n(t)$$

$$= -\sum_n \left[\frac{e^2 E_{\mathrm{f}}^2}{8\gamma m\omega^2} \{ e^{-i(\omega_{n-2} t - k_{n-2} z - 2\phi_0)} + e^{-i(\omega_{n+2} t - k_{n+2} z + 2\phi_0)} \} - \frac{e^2 E_{\mathrm{f}}^2}{4\gamma m\omega^2} e^{-i(\omega_n t - k_n z)} \right] a_n(t).$$

In the first two terms we shift the dummy index n: $n \to n \pm 2$ to finally find:

$$= -\frac{e^2 E_f^2}{4\gamma m\omega^2} \sum_n [\frac{1}{2}\{ a_{n+2}(t) e^{i2\phi_0} + a_{n-2}(t) e^{-i2\phi_0} \} - a_n(t)] e^{-i(\omega_n t - k_n z)}. \tag{S8}$$

Substituting the results given by Eq. S5, Eq. S7 and Eq. S8, we obtain the general tight-binding-approximated equation of motion:

$$\left[i\hbar \frac{\partial}{\partial t} + n\hbar(\omega - v_0 k_z) - n^2 \frac{(\hbar k_z)^2}{2m} + U_{\mathrm{p}} \right] a_n(t)$$

$$= \delta \left((k_{n+1} - \frac{k_z}{2}) a_{n+1}(t) e^{i\phi} + (k_{n-1} + \frac{k_z}{2}) a_{n-1}(t) e^{-i\phi} \right) \tag{S9}$$

$$- \frac{U_{\mathrm{p}}}{2} \left(a_{n+2}(t) e^{i2\phi_0} + a_{n-2}(t) e^{-i2\phi_0} \right),$$

where $\phi = \phi_0 + \frac{\pi}{2}$. We stress that the linear on-site potential term $n\hbar(\omega - v_0 k_z)$ stems from the phase mismatching, and the quadratic on-site potential term $n^2 \frac{(\hbar k_z)^2}{2m}$ originates from the electron dispersion curvature. The nearest-neighbor coupling term $\delta = e\hbar E_{\mathrm{f}}/(2m\omega)$ is laser induced, and $\pm\frac{k_z}{2}$ originates from the gauge contribution of $\nabla \cdot A \neq 0$. Lastly, the next-nearest-neighbor coupling showing the two-photon scattering process is proportional to the ponderomotive energy $U_{\mathrm{p}} = e^2 E_{\mathrm{f}}^2/(4m\omega^2)$.

We recall that in Wannier space which describes PINEM-type spectra we found the simplified equation of motion:

$$i\hbar \frac{\partial}{\partial t} a_n = (\kappa a_{n+1} + \kappa^* a_{n-1}) + \beta n^2 a_n. \tag{S10}$$

with the parameters κ, β. From this tight-binding Schrödinger equation, we wish to find the Hamiltonian, therefore we first span the slowly rotating wavevector using the PINEM ladder basis:

$$|\psi(t)\rangle = \sum_n a_n(t)|n\rangle.$$

We notice we can simply read off our tight-binding Hamiltonian directly from Eq. S10:

$$\hat{H} = \sum_n \beta n^2 |n\rangle\langle n| + (\kappa|n\rangle\langle n+1| + c.c). \tag{S11}$$

2 The Raman-Nath regime: multi-level Rabi model

We recall the form of Eq. S10 as the general tight-binding-approximated equation:

$$i\hbar \dot{a}_n(t) = \epsilon n^2 a_n + \kappa a_{n+1} - \kappa^* a_{n-1},$$

where $\epsilon = \frac{p_z^2}{2m}$ is the energy of a plane wave with momentum p_z. In the Raman-Nath regime we find $|\kappa| \gg \epsilon$. Therefore when treating ϵ as a perturbation, the unperturbed equation reads:

$$i\hbar\dot{a}_n(t) = \kappa a_{n+1} - \kappa^* a_{n-1}. \tag{S12}$$

We now wish to solve for Eq. S12, to do so we apply the phase transformation on Eq. S12: $\tilde{a}_n(t) = a_n e^{in(\phi_0 + \frac{\pi}{2})}$:

$$|\kappa| e^{i(\phi_0 + \frac{\pi}{2})} a_{n+1} = |\kappa| e^{i(\phi_0 + \frac{\pi}{2})} \tilde{a}_{n+1} e^{-i(\phi_0 + \frac{\pi}{2})} e^{-in(\phi_0 + \frac{\pi}{2})} = |\kappa| \tilde{a}_{n+1} e^{-in(\phi_0 + \frac{\pi}{2})},$$

$$|\kappa| e^{-i(\phi_0 + \frac{\pi}{2})} a_{n-1} = |\kappa| e^{-i(\phi_0 + \frac{\pi}{2})} \tilde{a}_{n-1} e^{i(\phi_0 + \frac{\pi}{2})} e^{in(\phi_0 + \frac{\pi}{2})} = |\kappa| \tilde{a}_{n-1} e^{in(\phi_0 + \frac{\pi}{2})}.$$

Thus by multiplying Eq. S12 by $e^{in(\phi_0 + \frac{\pi}{2})}$ we find

$$i\hbar\dot{\tilde{a}}_n = |\kappa|(\tilde{a}_{n+1} + \tilde{a}_{n-1}).$$

Implementing a $\frac{\pi}{2}$ phase shift yields

$$-\frac{i\hbar}{|\kappa|}\dot{\tilde{a}}_n = (\tilde{a}_{n-1} - \tilde{a}_{n+1}). \tag{S13}$$

From Eq. S13 we find the probability amplitude coefficients uphold the Bessel function recurrence relation

$$J_{n-1} - J_{n+1} = 2J_n',$$

i.e.,

$$\tilde{a}_n = J_n\left(\frac{2|\kappa|}{i\hbar}t\right).$$

Finally, we obtain the expression for a typical PINEM-type spectrum,

$$\boldsymbol{a_n = J_n\left(\frac{2|\kappa|}{i\hbar}t\right) e^{in\phi_0}}. \tag{S14}$$

3 Slow electron energy-momentum conservation condition

We begin by Taylor expanding the relativistic electron dispersion to second order:

$$E = \sqrt{c^2 p^2 + (mc^2)^2}. \tag{S15}$$

Here E, p, m are electron total energy, momentum and mass, respectively, and c is the speed of light. We first evaluate first and second derivatives of E at the initial momentum (velocity) p_0 (v_0):

$$\frac{\partial E}{\partial p}\bigg|_{p_0} = \frac{2c^2 p}{2\sqrt{c^2 p^2 + (mc^2)^2}}\bigg|_{p_0} = \frac{c^2 p_0}{E_0} = \frac{c^2 \gamma m v_0}{E_0} = v_0.$$

$$\frac{\partial^2 E}{\partial p^2} = c^2\left(\frac{1}{E} - p\frac{1}{E^2}\frac{\partial E}{\partial P}\right) = c^2\left(\frac{1}{E} - p\frac{1}{E^2}\frac{c^2 p}{E}\right) = c^2\left(\frac{1}{E} - p\frac{v}{E^2}\right).$$

$$\rightarrow \frac{\partial^2 E}{\partial p^2}\bigg|_{p_0} = c^2\left(\frac{1}{\gamma m c^2} - \gamma m v_0 \frac{v_0}{(\gamma m c)^2}\right) = \frac{1}{\gamma m}\left(1 - \left(\frac{v}{c}\right)^2\right) = \frac{1}{\gamma^3 m}.$$

We obtain the Taylor expansion

$$E \sim E_0 + v_0(p - p_0) + \frac{(p - p_0)^2}{2m\gamma^3} + \mathcal{O}((p - p_0)^3) \quad \text{for} \quad p \rightarrow p_0,$$

where γ is the Lorentz factor, $\gamma = \frac{1}{\sqrt{1-\beta}}$, and $\beta = \frac{v}{c}$.

5

Recalling from our Floquet-Bloch ansatz that $k_n = k_0 + nk_z$, we can rewrite $p - p_0$ as:

$$E = E_0 + vn\hbar k_z + \frac{(vn\hbar k_z)^2}{2\gamma^3 m}. \tag{S16}$$

From Eq. S16 we clearly see the physical origin of the quadratic potential. It emerges from the finite curvature of the electronic dispersion which is accessible for slow phase-matched electrons.

Park et al. [1] found that the energy-momentum conservation constraint for electron-electric field interactions manifests as

$$\cos(\theta_c) = \frac{2\hbar\omega E + (\hbar\omega)^2 - (\hbar k c)^2}{2\hbar k c^2 p},$$

where $\hbar k$ is the recoil momentum magnitude and θ_c is the critical angle, defined such that energy conservation at the single photon exchange between the light field and the electron is maintained, i.e. $E + \hbar\omega = \sqrt{c^2(\vec{p} + \vec{p}_{\text{photon}})^2 + (mc^2)^2}$ holds. Here the photon momentum is $\vec{p}_{\text{photon}} = (\hbar k \cos(\theta), \hbar k \sin(\theta))$. For a swift electron, e.g. $E = 200\,\text{keV}$, the interaction with a field with photon energy $\hbar\omega = 1.54\,\text{eV}$ yields $\frac{E}{\hbar\omega} \approx 10^5$. Thus, $2\hbar\omega E \gg (\hbar\omega)^2 - (\hbar k c)^2$ and we find the known energy-momentum conservation condition for the fast electron:

$$\frac{2\hbar\omega E}{2\hbar k c^2 p} = \frac{v_p}{v} \leq 1, \tag{S17}$$

where v_p is the optical field's phase velocity. Thus, conservation of energy and momentum has been reduced to matching the photon phase velocity and electron group velocity.

For a slow electron, e.g. $E = 100\,\text{eV}$, interacting with the same field we find $\frac{E}{\hbar\omega} \approx 10^2$. Therefore we keep the additional terms to find a correction for the slow electron energy-momentum conservation condition,

$$\cos(\theta_c) = \frac{2\hbar\omega E + (\hbar\omega)^2 - (\hbar k c)^2}{2\hbar k c^2 p} = \frac{2\hbar\omega E}{2\hbar k c^2 p} + \frac{(\hbar\omega)^2}{2\hbar k c^2 p} - \frac{(\hbar k c)^2}{2\hbar k c^2 p}.$$

Invoking the field phase velocity and electron group velocity we find

$$\boldsymbol{\cos(\theta_c) = \frac{v_p}{v}\left(1 + \frac{\hbar\omega}{2E}\left\{1 - \left(\frac{c}{v_p}\right)^2\right\}\right).} \tag{S18}$$

Equation S18 reveals that for the correction to be significant the electron's initial kinetic energy must be comparable to the photon energy due to the prefactor $\frac{\hbar\omega}{2E}$. Thus even for our slow electron with initial kinetic energy of $100\,\text{eV}$ the correction remains negligible.

4   When do $p \cdot A$ and ponderomotive terms become comparable?

In this section we theoretically study the ratio between the two terms for different field strengths interacting with a slow electron. To this end, we employ the simpler non-relativistic dispersion. The interaction between the electron and the electric field is given by the following Hamiltonian:

$$H = \frac{p^2}{2m} + \frac{epA}{m} + \frac{e^2 A^2}{2m}. \tag{S19}$$

We compare the $p \cdot A$ and ponderomotive term contributions for a slow electron with $50\,\text{eV}$ kinetic energy and an extremely slowly moving electron with $5\,\text{eV}$ energy. We examine the following field strengths: $0.09 - 10^3\,\text{V nm}^{-1}$. Our choice is motivated by commonly used and accessible field strength in typical experiments: $0.09 - 2\,\text{V nm}^{-1}$ are used in swift electron PINEM experiments, $10^2\,\text{V nm}^{-1}$ is the required field strength for ionizing hydrogen, and $10^3\,\text{V nm}^{-1}$ is employed in plasma physics. In addition, from Eq. S19 we find: $\frac{e^2 A^2}{2m_e} / \frac{epA}{m_e} = \frac{eA}{p}$. Therefore, in order to distinguish the dominant term we focus on the quantity $\frac{eA}{p}$.

E_{f} (V nm^{-1})	eA/p	
	$E = 50\,\mathrm{eV}$	$E = 5\,\mathrm{eV}$
0.09	$1.6 * 10^{-3}$	$5 * 10^{-3}$
2	$3.5 * 10^{-2}$	$1.1 * 10^{-1}$
10	$1.7 * 10^{-1}$	1.12
10^2	1.7	$1.12 * 10$
10^3	$1.77 * 10$	$1.12 * 10^2$

We find that for a $50\,\mathrm{eV}$ electron, even at field strengths on the order of $10^3\,\mathrm{V\,nm^{-1}}$ the ponderomotive term is only larger by an order of magnitude compared to the $p \cdot A$ term. At the atomic ionization field strength $10^2\,\mathrm{V\,nm^{-1}}$ they are of equal contribution, and for $1\,\mathrm{V\,nm^{-1}}$ the ponderomotive term can be treated as a perturbation. In addition, we find that as the electron becomes slower, e.g. at $5\,\mathrm{eV}$ kinetic energy which is on the order of the photon energy of $1.54\,\mathrm{eV}$, lower field strengths are needed for the ponderomotive term to have stronger contribution. For example, for a $5\,\mathrm{eV}$ electron a relatively weak field strength of $0.1\,\mathrm{V\,m^{-1}}$ already elevates the ponderomotive term to the extent of a perturbation which is two orders of magnitude weaker then the field strength required for the same effect for a $50\,\mathrm{eV}$ electron.

5 Non-symmetric Bloch oscillations

From Eq. S9 we find that when there is phase mismatching, i.e. $\hbar\omega \neq \hbar v_0 k_z$, the dominant on-site potential is the linear one. Therefore, the electron experiences a constant "field" in the energy domain leading to the emergence of Bloch-like oscillations. We find the oscillations are inherently non-symmetric for the slow electron from a simulation (see Fig. S1).
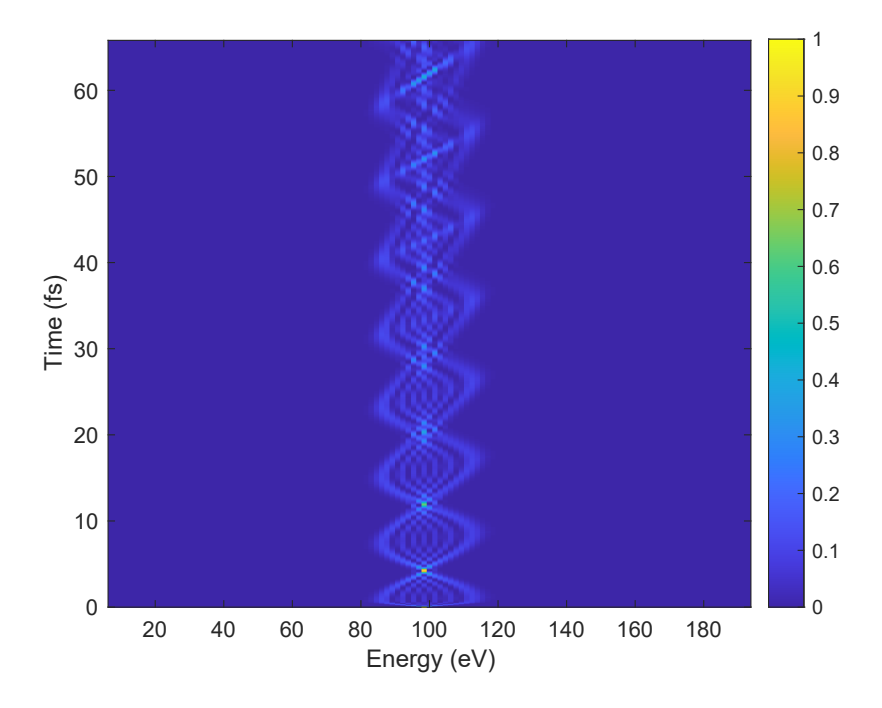

Figure S1: Slow electron non-symmetric Bloch oscillations in the energy domain. Field parameters: $E_{\mathrm{f}} = 1\,\mathrm{V\,nm^{-1}}$, $\phi_0 = 0$, $\hbar\omega = 1.54\,\mathrm{eV}$. The electron's kinetic energy is $100\,\mathrm{eV}$. A DLA grating with a period length of $\lambda_z \approx 23\,\mathrm{nm}$ introduces phase mismatching.

From the simulation we clearly see an asymmetry evolving with time between absorption and emission side bands. This asymmetry emerges as the maximal occupied absorption band is larger then the corresponding

7

emission band. This effect leads to a certain time delay between the time period of a single oscillation for absorption and emission bands.

References

[1] S. T. Park, M. Lin, and A. H. Zewail, Photon-induced near-field electron microscopy (PINEM): theoretical and experimental, New J. Phys. 12, 123028 (2010).